

# Hippocampal Remapping after Partial Inactivation of the Medial Entorhinal Cortex

## Highlights

- Partial inactivation of medial entorhinal cortex causes remapping in the hippocampus
- Inactivation-induced remapping is instantaneous
- Similar remapping was obtained with pharmacogenetic and optogenetic approaches
- Place cells maintain spatial firing properties after partial entorhinal inactivation

## Authors

Chenglin Miao, Qichen Cao, Hiroshi T. Ito, Homare Yamahachi, Menno P. Witter, May-Britt Moser, Edvard I. Moser

## Correspondence

chenglin.miao@ntnu.no (C.M.),  
edvard.moser@ntnu.no (E.I.M.)

## In Brief

Using pharmacogenetics and optogenetic methods, Miao et al. show that partial inactivation of the medial entorhinal cortex causes remapping among place cells in the CA3 area of the hippocampus. The size of individual place fields remains unaffected.

# Hippocampal Remapping after Partial Inactivation of the Medial Entorhinal Cortex

Chenglin Miao,<sup>1,\*</sup> Qichen Cao,<sup>1</sup> Hiroshi T. Ito,<sup>1</sup> Homare Yamahachi,<sup>1</sup> Menno P. Witter,<sup>1</sup> May-Britt Moser,<sup>1</sup> and Edvard I. Moser<sup>1,\*</sup>

<sup>1</sup>Kavli Institute for Systems Neuroscience and Centre for Neural Computation, Norwegian University of Science and Technology, Olav Kyrres Gate 9, Norwegian Brain Centre, 7489 Trondheim, Norway

\*Correspondence: chenglin.miao@ntnu.no (C.M.), edvard.moser@ntnu.no (E.I.M.)

<http://dx.doi.org/10.1016/j.neuron.2015.09.051>

## SUMMARY

Hippocampal place cells undergo remapping when the environment is changed. The mechanism of hippocampal remapping remains elusive but spatially modulated cells in the medial entorhinal cortex (MEC) have been identified as a possible contributor. Using pharmacogenetic and optogenetic approaches, we tested the role of MEC cells by examining in mice whether partial inactivation in MEC shifts hippocampal activity to a different subset of place cells with different receptive fields. The pharmacologically selective designer Gi-protein-coupled muscarinic receptor hM4D or the light-responsive microbial proton pump archaerhodopsin (ArchT) was expressed in MEC, and place cells were recorded after application of the inert ligand clozapine-N-oxide (CNO) or light at appropriate wavelengths. CNO or light caused partial inactivation of the MEC. The inactivation was followed by substantial remapping in the hippocampus, without disruption of the spatial firing properties of individual neurons. The results point to MEC input as an element of the mechanism for remapping in place cells.

## INTRODUCTION

The neuroscience of memory entered the modern era when Scoville and Milner reported, more than 50 years ago, that surgical removal of the hippocampi caused a severe disruption of memory for daily-life events (Scoville and Milner, 1957). Studies in animals and human subjects during the subsequent decades showed that the hippocampus is necessary for long-term memory of experience and facts, collectively referred to as declarative memory (Squire, 1992; Eichenbaum, 2000; Nadel et al., 2000). It is only more recently, however, that experiments have started to uncover the neural mechanisms of hippocampal memory formation.

A major advance in the search for hippocampal memory mechanisms was the discovery of place cells (O'Keefe and Dos-

trovsky, 1971). Place cells are cells that fire specifically when an animal is at a certain position in the environment. Different place cells fire at different positions, such that, collectively, the cells form a map-like dynamic representation of the moving animal's position (O'Keefe, 1976; O'Keefe and Nadel, 1978). However, place cells do not only represent the animal's current location. They may also reflect memory of a location, expressed as position-correlated firing patterns in the absence of the sensory inputs that originally elicited the firing (O'Keefe and Speakman, 1987; Jarosiewicz and Skaggs, 2004; Leutgeb et al., 2005a), or as an influence of past or future trajectories on the firing rates of place cells within their place fields (Wood et al., 2000; Frank et al., 2000; Fibreinteanu and Shapiro, 2003; Ito et al., 2015). Expression of memory in place cells is also apparent when place cells develop associations with reward-predictive stimuli (Komorowski et al., 2009; Igarashi et al., 2014) or when spatial firing patterns during foraging are subsequently replayed when the animal is resting (Pavlides and Winson, 1989; Wilson and McNaughton, 1994). The ability of place cells to express locations experienced in the past points to place cells as part of the mechanism for representation of experience in the hippocampus.

One indication of a link between place cells and memory is the existence of large numbers of apparently independent spatial representations, or maps, in the hippocampus (Colgin et al., 2008; Alme et al., 2014). Transitions between such representations are referred to as "remapping" (Muller and Kubie, 1987; Muller et al., 1991). Under some conditions, place cells completely change their firing patterns in response to relatively minor alterations in sensory or motivational inputs (Muller and Kubie, 1987; Markus et al., 1995). Following changes in the configuration or location of an environment, place fields may appear, disappear, or move to new locations. Under these circumstances, the new pattern of activity may be no more similar to the original pattern than expected by chance (Leutgeb et al., 2004). This nearly complete orthogonalization of hippocampal place maps for different environments ("global remapping") is thought to enable storage of discrete representations, with minimal risk of interference (Battaglia and Treves, 1998; Colgin et al., 2008).

The mechanism of hippocampal remapping has not been determined. Activity changes in the hippocampus can be elicited by a number of cortical and subcortical inputs. One of these is

the projection from medial entorhinal cortex (MEC), which comprises axons from a variety of spatially modulated cell types, including grid cells and border cells (Hafting et al., 2005; Solstad et al., 2008; Zhang et al., 2013). Remapping in hippocampal place cells could reflect changes in the firing pattern of these entorhinal cell types, such as a relative displacement of the firing locations of grid cells from different grid modules when the animal moves from one environment to another (Fyhn et al., 2007; Stensola et al., 2012). In agreement with this hypothesis, inactivation of the MEC appears to cause substantial change in the firing locations of hippocampal place cells in two studies (Ormond and McNaughton, 2015, their Figure S8; Rueckemann et al., 2015), although it is not clear whether this change reflects a switch to a new map or mere instability in the firing locations of the place cells. In the one study in which time course was estimated (Rueckemann et al., 2015), the change was slow and gradual, with a developmental trajectory very different from the sharp transition usually observed in response to salient changes in the environment (Muller and Kubie, 1987; Leutgeb et al., 2006). To determine the nature of the remapping, we recorded, on a lap-by-lap basis, the firing locations of place cells in hippocampal area CA3 after partial but specific inactivation of the MEC, using virus-assisted optogenetic or pharmacogenetic techniques for local neuronal silencing. If remapping is caused by changes in the pattern of simultaneously active MEC cells, remapping should be seen with both approaches after partial MEC inactivation. The study also gave us the opportunity to determine, with more specific interventions, the impact of MEC input on the formation of place fields in the hippocampus.

## RESULTS

### Strategy for Partial Inactivation of the MEC

To determine whether changes in MEC firing patterns cause remapping in hippocampal place cells, we silenced MEC cells in mice with tetrodes implanted at dorsal-to-intermediate levels of the CA3 area of the hippocampus (Figure 1). MEC neurons were silenced by local injection of an adeno-associated virus (AAV) expressing either the pharmacologically selective designer Gi-coupled muscarinic receptor hM4D (Armbuster et al., 2007) or the optogenetic silencer archaerhodopsin (ArchT) (Chow et al., 2010; Han et al., 2011). hM4D was fused with the fluorescent protein mCitrine; ArchT was fused with GFP. In 14 mice, AAV was injected in both dorsal and ventral MEC in order to cover the entire dorso-ventral length of the MEC (“global MEC infection,” 8 mice with hM4D and 6 mice with ArchT). In 6 mice, AAV was injected in dorsal MEC only (4 mice with hM4D and 2 mice with ArchT). In 3 mice, AAV was injected only in ventral MEC (hM4D). In addition, 3 mice received control injections of AAV-mCitrine ( $n = 2$ ) or AAV-GFP ( $n = 1$ ) at dorsal and ventral MEC locations.

To verify that MEC cells can be inactivated following expression of hM4D or ArchT, we implanted tetrodes within the infected area. Three weeks post-infection, we recorded entorhinal spike activity while the mice foraged randomly in a 1-m-wide square box (Figure 1A). Grid cells, border cells, and head direction cells were identified based on firing patterns in the box. We then recorded the same cells in a smaller box ( $30 \times 30$  cm) to maximize

coverage and to reduce recording time. In AAV-hM4D-infected animals, after 5 min baseline recording, the infected cells were hyperpolarized by i.p. injections of the hM4D-specific ligand clozapine-N-oxide (CNO) (Figure 1B). Thirty minutes later, activity in the small box was reduced to less than 50% of the baseline rate in 29 out of 35 MEC neurons. Mean firing rates were reduced from  $2.36 \pm 0.34$  Hz before CNO to  $0.71 \pm 0.24$  Hz 30 min after CNO (35 cells from 2 mice, Wilcoxon signed rank test,  $Z = 4.82$ ,  $p = 3.0 \times 10^{-5} < 0.0001$ , Figure 1C). The activity recovered toward baseline levels after 12 hr (mean firing rate,  $2.02 \pm 0.39$  Hz, Wilcoxon signed rank test,  $Z = 1.95$ ,  $p = 0.52$ ). In AAV-ArchT-infected animals, the MEC cells were inactivated by continuous laser application at a wavelength of 532 nm. Firing rates were reduced to less than 50% of the baseline rate in 22 out of 24 MEC neurons. Mean rates were reduced from  $1.30 \pm 0.26$  Hz before light application to  $0.28 \pm 0.11$  Hz 30 min after light (24 cells from 3 mice, Wilcoxon signed rank test,  $Z = 3.86$ ,  $p = 1.0 \times 10^{-4}$ , Figure 1F). All functional cell types were inhibited in both experiments (all 6 grid cells; 2 out of 3 border cells; 3 out of 4 and 4 out of 5 head direction cells, respectively; Figures 1A and 1D). mCitrine-hM4D expression was not observed in hippocampal cell bodies, only in bypassing axons (10 mice; 6–16 sections per animal; Figures S3A–S3C), suggesting that the effect of CNO was largely restricted to the injection area in the MEC. GFP-ArchT was seen in CA2 in 2 out of 8 mice with ArchT expression; in the remaining mice, no expression was detected in cells with cell bodies in the hippocampus (Figures S3D–S3F).

To estimate the extent of MEC inactivation with a different method, we compared the number of c-Fos-positive cells after CNO injection on the injection side with the number on the contralateral side in animals with unilateral AAV-hM4D injections. Cells were counted within randomly selected frames in MEC (Figure S5). The density of c-Fos-positive cells on the AAV-hM4D-infected side of MEC was significantly lower than on the uninfected contralateral side ( $19.2\% \pm 4.0\%$  versus  $43.8\% \pm 11.9\%$  of MEC cells, Mann-Whitney U test,  $Z = 2.19$ ,  $p = 0.028$ ). The reduction of MEC activity after local silencing validates the hM4D intervention as a strategy for partial silencing of the MEC.

### Spatially Selective Firing Is Maintained in the Hippocampus after Partial MEC Inactivation

We first examined how individual place cells respond to changes in the pattern of simultaneously active cells in the MEC. AAV-hM4D-mCitrine was injected across multiple dorso-ventral levels of MEC in 15 mice with tetrodes in hippocampal area CA3. In animals with both dorsal and ventral injections, mCitrine-expressing cells could be observed across the entire dorso-ventral range of MEC (Figure 2). In dorsally injected animals, expression was limited to the dorsal half, whereas after ventral injections, it was limited to the ventral part. On average, mCitrine was expressed across  $49.0\% \pm 17.8\%$  of the MEC (mean  $\pm$  SEM.; individual estimates range between 23.1% and 78.3%; Figure S1 and Table S1). On average,  $18.7\% \pm 6.6\%$  of the infection volume was in neighboring regions, including lateral entorhinal cortex ( $4.3\% \pm 4.0\%$  of the part of lateral entorhinal cortex that was present in sections containing MEC; see Experimental Procedures), presubiculum ( $7.0\% \pm 6.8\%$  of this

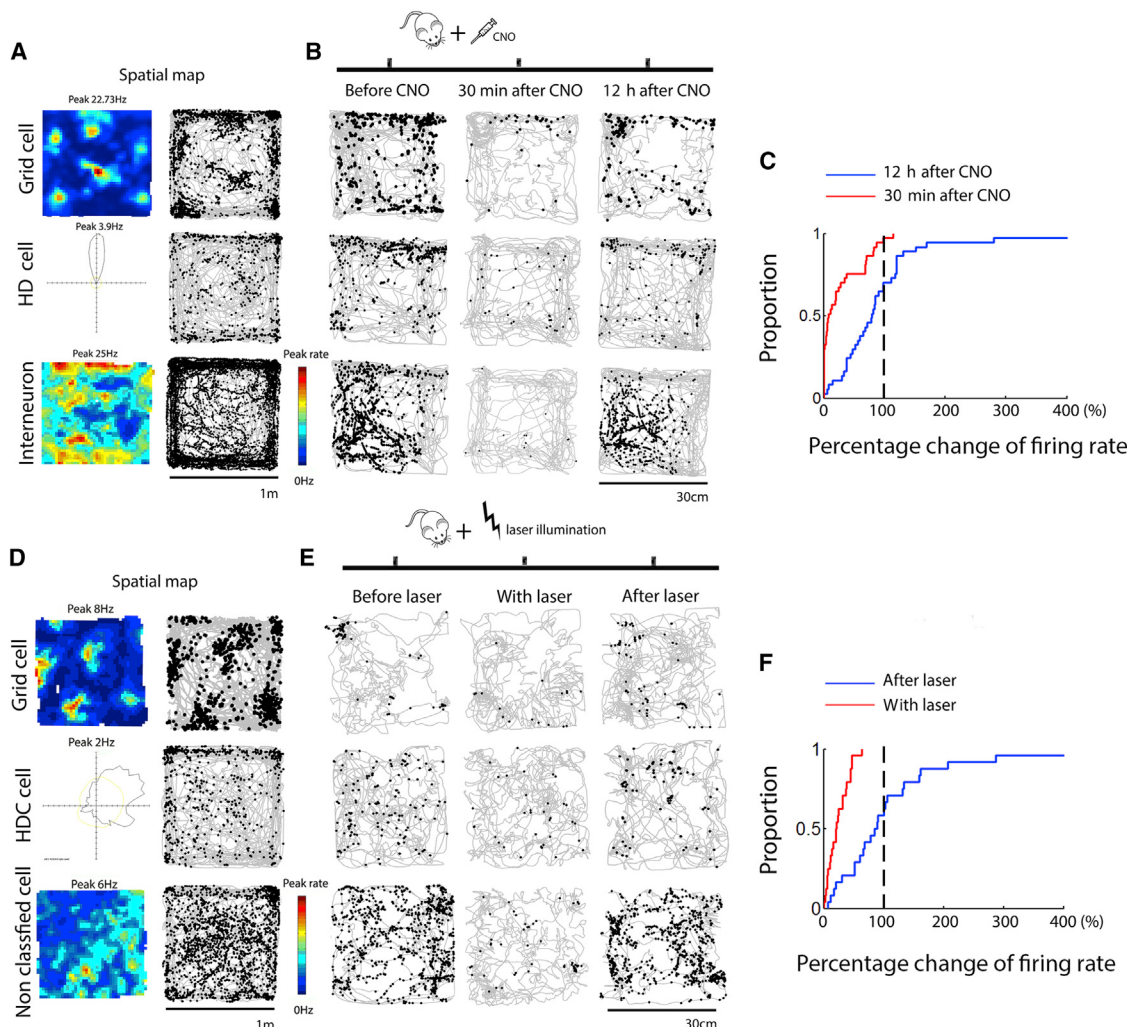


**Figure 1. Inhibition of MEC Activity with hM4D and ArchT**

(A) Spatial map of MEC cells recorded during foraging in a 1 m square box (grid cell, head direction cell, and interneuron). Left: color-coded rate maps; color scale to the right. Right: trajectory (gray) with spike positions superimposed (black). The cells were from mice with hM4D expression in MEC.

(B) Same cells as in (A) recorded before CNO, 30 min after CNO, and 12 hr after CNO in a 30 cm square box (note scale change from A). Spikes are superimposed on the trajectory as in (A).

(C) Cumulative frequency diagrams showing percentage change in firing rate 30 min and 12 hr after CNO compared to baseline ( $n = 37$ ). Stippled line indicates no change (100% of baseline level).

(D) Spatial map of a different set of MEC cells in the 1 m square box. The cells were recorded in mice with ArchT expression in MEC.

(E) Spike activity of MEC cells in (D) before, during, and after laser illumination in the 30 cm square box (5 min each session).

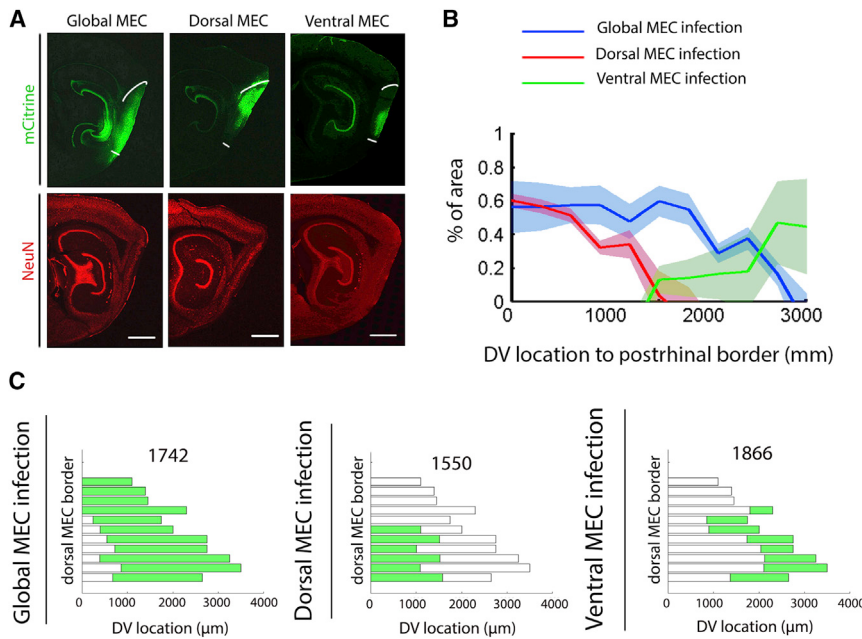
(F) Cumulative frequency diagrams showing change in firing rate during and after laser stimulation compared to baseline ( $n = 24$ ). Symbols are as in (C).

area), and parasubiculum ( $12.2\% \pm 8.1\%$ ), postrhinal cortex ( $13.0\% \pm 11.8\%$ ), subiculum ( $2.0\% \pm 2.9\%$ ), and dentate gyrus ( $0.2\% \pm 0.1\%$ ). Within the infected area, the large majority of the cells, probably more than 90%, were hM4D-mCherry positive (Figures S2A–S2D).

Place cells were recorded from CA3 while the mice ran a minimum of ten laps on a 1-m-long linear track. Running was rewarded by chocolate crumbs at the ends of the track. We restricted our analysis to cells with stable location-selective activity on the baseline sessions (spatial correlation of first and second halves of the session  $> 0.5$ ). 41 out of 139 cells (30%) expressed stable loca-

tion-selective activity at least in one running direction on the track. 34 of them (24%) expressed firing fields in both running directions. Because most of these cells fired at different locations on left and right runs (spatial correlation:  $0.252 \pm 0.028$ ; peak position difference:  $15.3 \pm 2.2$  cm, peak rate difference [low/high]:  $0.48 \pm 0.04$ ; mean  $\pm$  SEM), as reported previously (McNaughton et al., 1983), we treated run directions as distinct datasets (Table S2). The total number of datasets was 109.

Inactivation of MEC with the hM4D ligand CNO had minimal impact on the spatial firing properties of individual place cells in hM4D-expressing animals (Figures 3 and S6). There was a

**Figure 2. Distribution of MEC Infection**

(A) Expression of hM4D-GFP in MEC after AAV-hM4D infection across large parts of the MEC (left), in dorsal MEC only (middle), or in ventral MEC only (right). Dorsal and ventral borders of MEC are indicated by white lines. NeuN stains of adjacent sections are shown to indicate distribution of cell bodies in all regions. Scale bar, 1,000  $\mu$ m.

(B) Percentage of MEC area with mCitrine expression for mice with widespread AAV-hM4D injections or injections only in dorsal or ventral MEC.

(C) Unfolded “flat” maps of MEC showing the outline of the transfected area in example mice with global transfection (both dorsal and ventral MEC) or only dorsal or ventral MEC.

significant reduction of the mean firing rate of the place cells (before CNO,  $3.83 \pm 0.42$  Hz; 30 min after CNO,  $2.81 \pm 0.33$ ; Wilcoxon signed rank test  $Z = 4.06$ ,  $p = 4.9 \times 10^{-5}$ ) (Figure 3C), but there were no significant changes in spatial firing properties such as spatial information content (before CNO:  $0.85 \pm 0.06$  bits/spike; 30 min after CNO,  $0.83 \pm 0.07$  bits/spike, Wilcoxon signed rank test  $Z = 0.697$ ,  $p = 0.49$ ; Figure 3D) or the number of firing fields per cell (before CNO:  $1.12 \pm 0.03$ ; 30 min after CNO:  $1.02 \pm 0.05$ ; Wilcoxon signed rank test,  $Z = 1.52$ ,  $p = 0.127$ ). The size of the place fields was estimated by constructing, for all cells in the experimental group, a cross-correlation matrix of pairs of population vectors for firing rates along successive bins of the track (20 bins in total; 4 cm each; Figures 3E–3H). The mean distance from the diagonal of the matrix to population vectors with a mean correlation of 0.2 was considered as the effective size of the place fields (Ormond and McNaughton, 2015). Place field size was not significantly changed after CNO ( $r = 0.2$  threshold before CNO:  $4.65 \pm 0.49$  bins; 30 min after CNO:  $4.80 \pm 0.65$  bins,  $p = 0.85$ ;  $p$  value was estimated from bootstrap distributions) (Figures 3E–3H). The lack of effect on size of place fields was threshold independent (Figure 3H). There was no significant change in the running speed of the animal after CNO (before:  $24.2 \pm 0.66$  cm/s, 30 min after:  $23.3 \pm 0.85$  cm/s, Wilcoxon signed rank test,  $Z = 1.465$ ,  $p = 0.143$ ).

There was only minimal difference in place field properties of mice with hM4D expression limited to either dorsal or ventral MEC. Mean firing rates were reduced significantly after CNO in the ventral injection group (before CNO,  $5.70 \pm 0.99$  Hz; 30 min after CNO,  $3.36 \pm 0.62$  Hz; Wilcoxon signed rank test  $Z = 3.80$ ,  $p = 1.43 \times 10^{-4}$ ) but not in mice with dorsal injections (before CNO,  $3.41 \pm 0.88$  Hz; 30 min after CNO,  $3.23 \pm 0.67$  Hz; Wilcoxon signed rank test  $Z = 0.315$ ,  $p = 0.75$ ). There was no change in the spatial firing properties of place fields in either group. Spatial information was unaltered (dorsal group before CNO:  $1.02 \pm 0.15$  bits/spike; 30 min after CNO,  $0.87 \pm 0.13$  bits/spike, Wilcoxon

signed rank test  $Z = 0.545$ ,  $p = 0.586$ ; ventral group before CNO:  $0.64 \pm 0.07$  bits/spike; 30 min after CNO,  $0.77 \pm 0.10$  bits/spike, Wilcoxon signed rank test  $Z = 0.898$ ,  $p = 0.339$ ). There was no change in the population vector cross-correlation matrices used to determine field size (distance from diagonal in the dorsal group: before CNO:  $5.14 \pm 0.39$  bins; 30 min after CNO:  $4.90 \pm 0.45$  bins,  $p = 0.82$ ; distance from the diagonal in the ventral group before CNO:  $6.25 \pm 0.75$  bins; 30 min after CNO:  $5.07 \pm 0.57$  bins,  $p = 0.19$ ;  $p$  values were estimated from bootstrap distributions) (Figures 5E and 5J).

### Hippocampal Remapping after Partial MEC Inactivation

CNO caused substantial remapping in the place-cell population (Figures 4 and S6; Tables S2–S5). Remapping was expressed in individual place cells as a drop in spatial correlation between rate maps for baseline trials and trials conducted with the same cells in the same environment 30 min after CNO (first versus second half of the baseline:  $r = 0.76 \pm 0.013$ ; 30 min after CNO versus baseline:  $r = 0.41 \pm 0.045$ , paired sample t test after Fisher z-transformation,  $t(108) = 6.41$ ,  $p = 4.08 \times 10^{-9}$ ). The spatial correlation was still reduced 12 hr after CNO (12 hr after versus baseline:  $0.46 \pm 0.038$ , paired sample t test  $t(108) = 7.17$ ,  $p = 9.84 \times 10^{-11}$ ), although the firing fields at 12 hr correlated more strongly with the baseline pattern than with the pattern 30 min after CNO ( $r = 0.36 \pm 0.038$ ; paired sample t test after Fisher z-transformation,  $t(108) = 2.41$ ,  $p = 0.018$ ). For cells expressing place fields in both running directions, the amount of remapping, measured by spatial correlation between baseline and the CNO trial, was positively correlated between inbound and outbound place fields ( $R = 0.616$ ,  $p = 0.002$ ). A similar drop in correlation during CNO was not present in AAV-GFP-infected control mice, despite widespread GFP expression (mean correlation:  $0.77 \pm 0.03$ ,  $n = 18$ ; two-sample t test  $t(125) = 2.88$ ,  $p = 0.005$ , Figure 4B). The drop in spatial correlations after CNO injection in the hM4D group was accompanied by a significant shift of the center of mass of the place fields compared to the first versus second half of the baseline session (mean  $\pm$  SEM:  $12.8 \pm 1.4$  cm versus  $5.5 \pm 0.72$  cm; Wilcoxon signed rank test,  $Z = 4.869$ ,  $p = 1.0 \times 10^{-6}$ ).

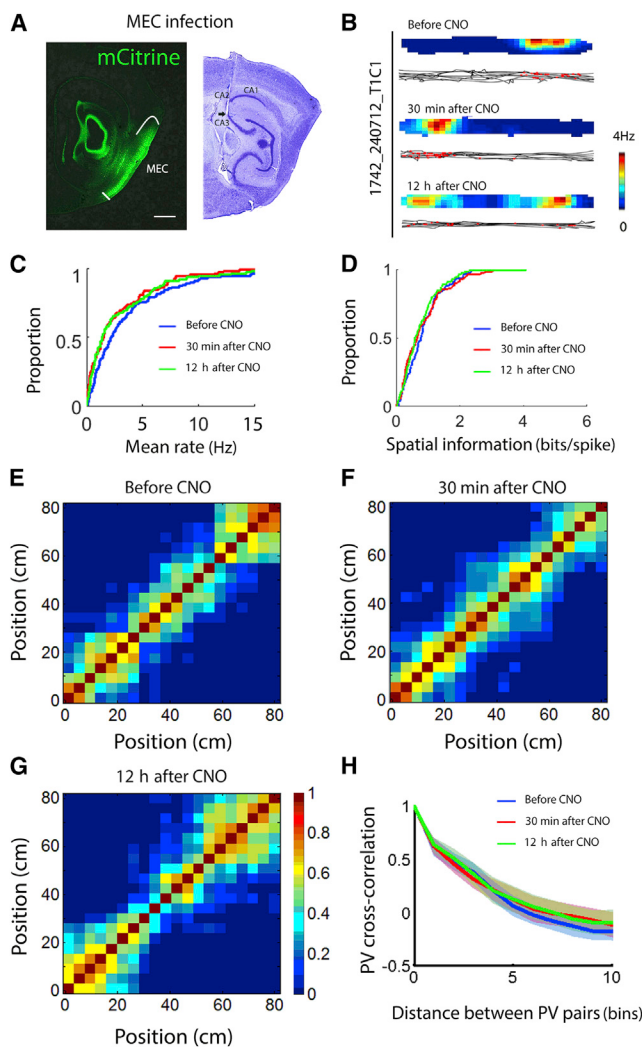


**Figure 3. Partial Inactivation of MEC Did Not Change the Firing Properties of Place Cells**

(A) Left: sagittal brain section showing expression of hM4D-mCitrine(Green) across a substantial part of the dorsoventral MEC axis. Dorsal and ventral borders of MEC are indicated by white lines. Expression is also seen in axonal projections into the hippocampus to the left of the MEC. Scale bar, 800  $\mu$ m. Right: Nissl-stained sagittal brain section showing position of tetrode (arrow) in the same animal.

(B) Color-coded rate maps showing firing locations of a representative CA3 place cell on the linear track before CNO, 30 min after CNO, and 12 hr after CNO. Color scale is to the right.

(C and D) Cumulative frequency diagrams showing no change in mean firing rate (C) or spatial information (D) of place fields after CNO in hM4D-expressing animals.

(E–G) Population vector cross-correlation matrices for the baseline trial (E), 30 min after CNO (F), and 12 hr after CNO (G). Analyses include all place cells from all animals in the experimental group.

(H) Overlaid decorrelation curves showing mean correlation (solid lines)  $\pm$  95% confidence intervals (shaded color) for each possible population vector pair distance between 0 and 10 bins (4 cm each bin). The confidence intervals were estimated by a bootstrap resampling procedure. To quantify the scale of the spatial representation, we calculated the distance at which the correlation dropped to  $r = 0.2$ . Note similar distances before, during, and after CNO.

The distribution of spatial correlations between firing before and after CNO was compared to a shuffled distribution obtained by random displacement of firing locations along the trajectory on the track of the animal together with random replacement of cell identities. The spatial correlation between the first half and the second half of the baseline session, before CNO, was significantly above the 95<sup>th</sup> percentile of the shuffled distribution for 101 out of 109 sets of place fields (94%) (Figure 4B), as expected given that cells were pre-selected for stability. After CNO application, the correlation with the baseline session dropped. Only 55 out of the 109 place fields (51%) had spatial correlation values that passed the 95<sup>th</sup> percentile of the shuffled distribution (baseline versus CNO,  $Z = 6.99$ ,  $p = 2.79 \times 10^{-12}$ ; binomial test). The low similarly to the baseline pattern was maintained 12 hr after CNO (55 place fields, or 51%, above the 95<sup>th</sup> percentile). A similar reduction was seen at 12 hr in control animals (12 out of 18 place fields, or 67%; CNO versus control, binomial test,  $Z = 1.27$ ,  $p = 0.20$ , Figure 4B), as expected given the low long-term stability of place fields in mice (Kentros et al., 2004).

At the neural ensemble level, there was a significant reduction after CNO in correlations between population vectors across bins of the linear track (bin size 4 cm, 20 bins in total; Figure 4B). Before CNO, all 20 population vector correlations were outside of the 95<sup>th</sup> percentile of a shuffled distribution (first versus second half of the baseline session). After CNO, only 14 correlations (70%) passed the 95<sup>th</sup> percentile threshold ( $Z = 2.66$ ,  $p = 0.008$ , binomial test compared to the baseline). The shift persisted 12 hr after CNO (16 correlations, or 80%, above the threshold). In control mice infected with AAV-GFP, all 20 correlations exceeded the 95<sup>th</sup> percentile threshold at 30 min, which is significantly above the level in the hM4D group ( $Z = 2.66$ ,  $p = 0.008$ , binomial test). At 12 hr, the number had dropped to 14 (70%). In agreement with these counts, the drop in population vector correlations at 30 min in the hM4D group was significantly larger than in the control group (mean correlations of  $0.18 \pm 0.02$  and  $0.74 \pm 0.04$ , respectively;  $t$  test for correlation values after Fisher z-transformation,  $t(38) = 9.49$ ,  $p = 1.43 \times 10^{-11}$ , Figure 4B). Taken together, the results show that partial inhibition of the MEC induces substantial change in the firing locations of place cell ensembles in the hippocampus.

The decrease in spatial correlations was observed also in the subgroup of animals with inactivation limited to the dorsal MEC (Figures 5A–5E and S1; first versus second half of the baseline: 24 out of 30 place fields passed the 95<sup>th</sup> percentile threshold; mean correlation value:  $0.77 \pm 0.028$ ; 30 min after CNO versus baseline: 16 out of 30 fields passed the threshold; mean correlation:  $0.50 \pm 0.08$ , binomial test,  $Z = 2.19$ ,  $p = 0.03$ ; paired sample  $t$  test for correlation values after Fisher z-transformation,  $t(29) = 3.04$ ,  $p = 0.005$ ). There was a small decrease in spatial correlation also after ventral MEC inactivation (Figures 5F–5J; first versus second half of the baseline: 25 out of 28 place fields passed the 95<sup>th</sup> percentile threshold; mean correlation value:  $0.79 \pm 0.022$ ; 30 min after CNO versus baseline: 20 out of 28 fields passed the threshold; mean correlation:  $0.64 \pm 0.06$ , binomial test,  $Z = 1.68$ ,  $p = 0.09$ ; paired sample  $t$  test for correlation values after Fisher z-transformation,  $t(27) = 2.30$ ,  $p = 0.03$ ). In the population vector analyses, there was a significant decrease in the number of bins passing the 95<sup>th</sup> percentile of the shuffled distribution

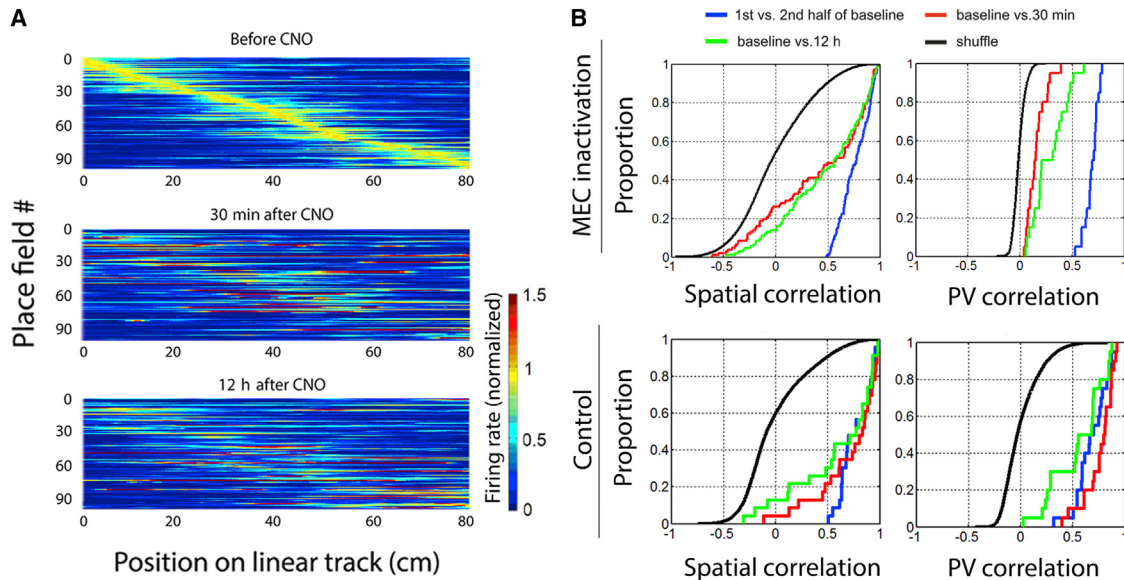


**Figure 4. Partial Inactivation of MEC Induced Remapping in CA3 Place Cells**

(A) Color-coded population map showing location of CA3 place fields before CNO, 30 min after CNO, and 12 hr after CNO. Each line shows activity of one place cell in one running direction (109 datasets in total from 75 place cells). Color indicates firing rate (scale bar to the right). Firing rate was normalized for each cell to the cell's baseline firing rate. The upper limit of the colour code is 1.5 times the peak firing rate of the cell in the baseline session; thus colour codes are saturated (red) in cells with larger rate changes. Cells are sorted according to position of the place field (center of mass) during the baseline trial. The sequence of cells is the same for all three plots (before CNO, 30 min after and 12 h after). Only cells with stable firing in the baseline session (spatial correlation between first and second half of the session > 0.5) are shown.

(B) Cumulative frequency distributions showing spatial correlations and population vector correlations for different pairs of epochs in the CNO experiment: first versus second half of the baseline period, 30 min post-CNO versus baseline, and 12 hr post-CNO versus baseline. Data are shown for all animals with hM4D expression in dorsal, ventral or dorsal-and-ventral MEC (top) as well as control animals with GFP expression only (bottom). Spatial correlation for shuffled pairs of distributions is shown for comparison.

30 min after CNO in the dorsal hM4D group (before CNO 20/20 bins; after CNO: 5 bins; binomial test,  $Z = 4.89$ ,  $p = 9.63 \times 10^{-7}$ ; Figure 5D). A similar reduction was not observed in mice with selective ventral MEC inhibition (before CNO: 20/20 bins; after CNO: 19/20 bins; binomial test,  $Z = 1.01$ ,  $p = 0.31$ ; Figure 5I).

We next asked whether the change in spatial firing patterns after CNO was instantaneous, as expected if a new ensemble pattern was recruited in the same way as when place cells remap in a novel environment. Alternatively, firing patterns might change gradually, as would be expected if the change was caused by instability in the hippocampal ensemble code (Ken-tros et al., 2004). To distinguish between these possibilities, we compared population vectors on each lap with the average of the baseline session. Because each session consisted of 10 laps or more, we selected the last 10 laps from the baseline session and the first 10 laps from the CNO session. In hM4D mice, we found that the population vector correlation with the baseline average was significantly lower on the first lap after CNO (the 11<sup>th</sup> lap) than on the last lap before CNO (Figure 6A; before:  $0.47 \pm 0.02$ ; after:  $0.22 \pm 0.03$ , t test for correlation values after Fisher z-transformation,  $t(38) = 6.93$ ,  $p = 3.11 \times 10^{-8}$ ). The correlation between the 11<sup>th</sup> lap and the average of the first 10 laps after CNO was significantly higher than the correlation with the average of the 10 preceding baseline laps ( $0.47 \pm 0.02$  versus  $0.30 \pm 0.02$ , t test for correlation values after Fisher z-transformation,  $t(38) = 4.89$ ,  $p = 1.86 \times 10^{-5}$ ) (Figure 6A). A simi-

larly sudden drop on the first lap after CNO was not observed in GFP control animals (Figure 6B). The abrupt change of the population vector correlation suggests that the place-cell population remapped instantaneously.

#### Remapping after Targeted Inhibition of MEC Projections

The pharmacogenetic study points to MEC, and particularly dorsal MEC, as a critical source of remapping in dorsal hippocampal place cells. To determine whether this influence is mediated by direct projections from MEC cells to the hippocampus, we used optogenetic methods to selectively inactivate MEC fibers within the hippocampus itself. ArchT-encoding AAV was infused in MEC and place cells were recorded in CA3, at the same septotemporal level as in the pharmacogenetic study, while continuous 532 nm laser light was applied through an optic fiber aimed at the perforant path (Figure S1; Figure 7A). ArchT-GFP was expressed across  $53.6\% \pm 11.9\%$  of the MEC (mean  $\pm$  SEM; individual estimates range between 35.3% and 70.4%; Figure S1 and Table S1). Only  $20.7\% \pm 7.5\%$  of infected volume was outside the MEC ( $4.2\% \pm 3.6\%$  of the lateral entorhinal cortex that was part of sections comprising MEC, see Experimental Procedures;  $5.3\% \pm 4.5\%$  of presubiculum,  $14.0\% \pm 6.0\%$  of parasubiculum,  $9.1\% \pm 5.5\%$  of postsubiculum, and  $3.8\% \pm 4.8\%$  of subiculum). Within the infected area, a large majority of the cells, probably over 90%, were ArchT-GFP positive (Figures S2E–S2H). The effect of ArchT-induced

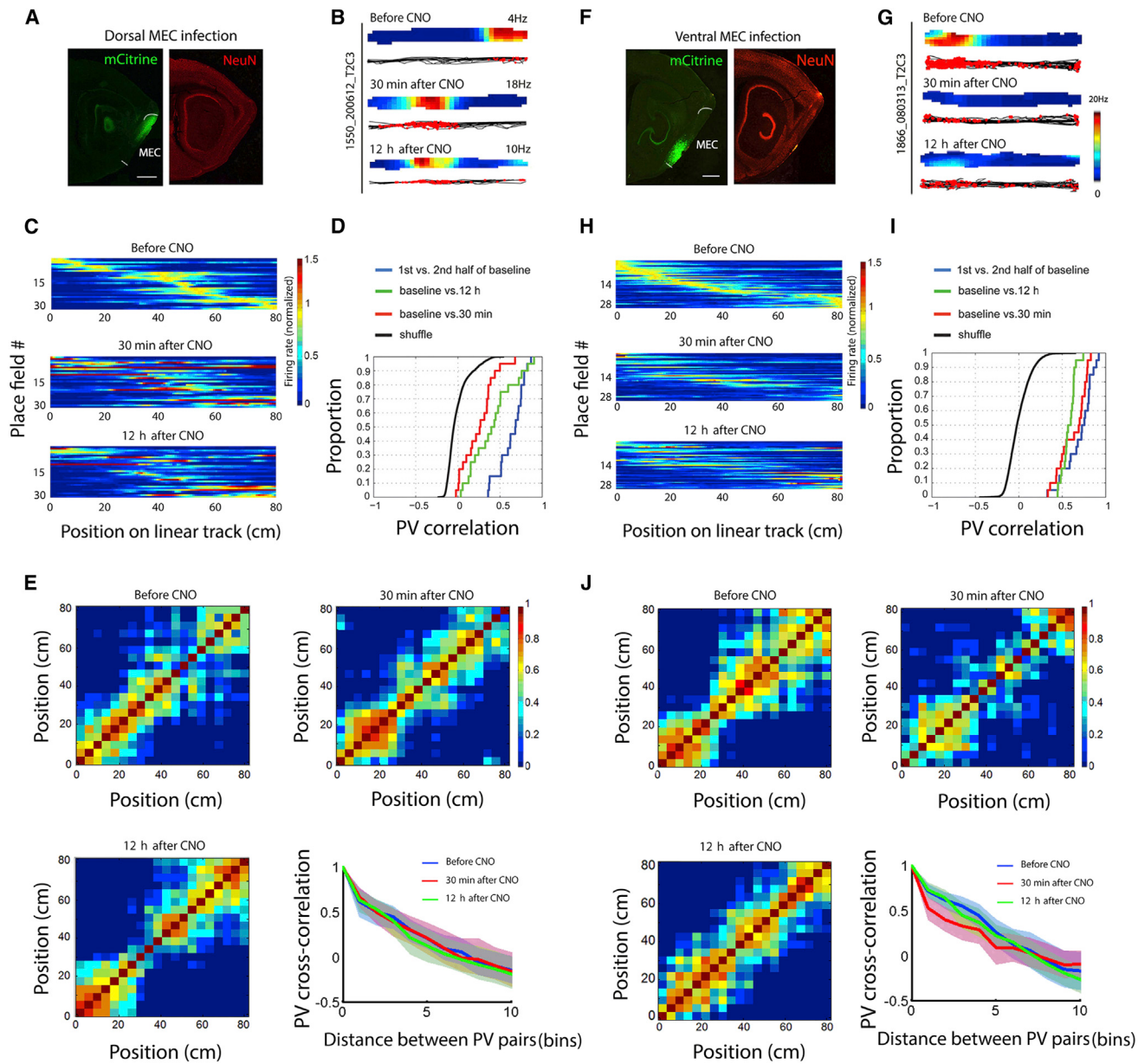


**Figure 5. Comparison of Dorsal and Ventral MEC Inactivation**

(A and F) Sagittal brain sections showing expression of hM4D-mCitrine(Green) in dorsal (A) and ventral (F) MEC, respectively, (left) and the same sections stained for NeuN (right). Scale bar, 800 μm.

(B and G) Color-coded rate maps showing firing locations of representative CA3 place cells on the linear track before CNO, 30 min after CNO, and 12 hr after CNO. Color scales are to the right.

(C and H) Color-coded population maps showing changes in firing locations of CA3 place fields after CNO. Dorsal MEC group (C): n = 30, ventral MEC group (H): n = 28. Symbols are as in Figure 4A.

(D and I) Cumulative frequency distributions showing population vector correlations between different epochs of the CNO experiment. Symbols as in Figure 4B.

(E and J) Population vector cross-correlation matrices from baseline, 30 min after CNO, and 12 hr after CNO. Decorrelation curves in the bottom right quadrants show similar mean distances for all possible population vector pairs at values up to 10 bins (4 cm each bin). Symbols as in Figures 3E–3H.

silencing was expressed in all types of spatial cells in the MEC, including grid cells, head direction cells, and non-classified spatial cells (Figures 1D–1F). Continuous laser illumination (3 to 5 min) in the hippocampus did not induce neural apoptosis at levels that were detectable in a TUNEL assay (Figures S3G–S3I).

In the 8 animals with ArchT expression in MEC, 56 out of 109 CA3 cells expressed stable location-selective activity on the track in the baseline session. 83 sets of stable place fields were obtained after combining run directions (Figures 7B–7E). The laser stimulation decreased the mean firing rate of

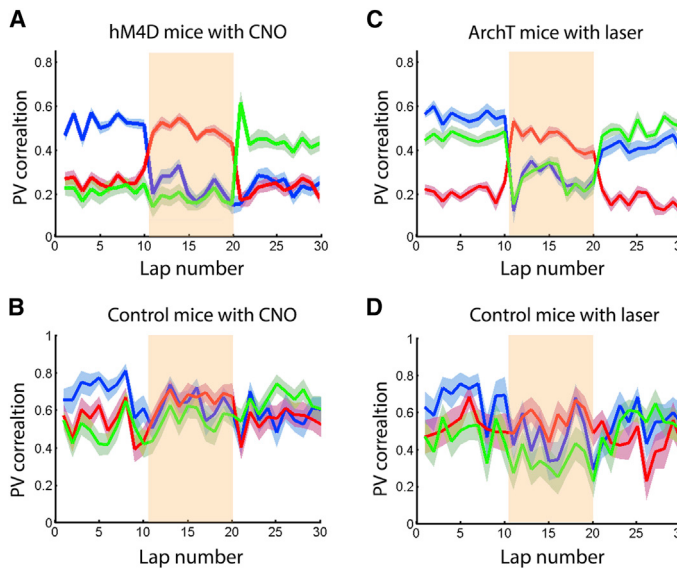


**Figure 6. Lap-by-Lap Analysis of Population Vectors**

The analysis includes a total of 30 laps (10 from the baseline, 10 from the MEC inactivation, and 10 from the recovery session). Population vectors were defined for each spatial bin of the linear track. Population vectors on individual laps were then correlated with the average of the last 10 laps of the baseline session (blue), the average of the first 10 laps of the MEC inactivation (red), or the average of the first 10 laps of the recovery session (green). Plots show mean population vector correlations across 20 spatial bins (solid lines) with SEM (shaded colors). (A) Lap-by-lap population vector correlations before and after CNO in mice injected with AAV-hM4D in MEC. (B) Similar correlations in control mice injected with AAV-GFP in MEC. (C) Lap-by-lap population vector correlations before and after light stimulation in mice injected with AAV-ArchT in MEC. (D) Laser stimulation in control mice injected with AAV-GFP. Note abrupt change in population vector correlations at the onset of MEC silencing. The change was not observed in control mice injected with CNO or laser illumination.

place cells in CA3 (before laser,  $3.18 \pm 0.44$  Hz; with laser,  $2.31 \pm 0.30$  Hz; Wilcoxon signed rank test,  $Z = 2.06$ ,  $p = 0.04$ ; Figure 7C). The rates in the ArchT group recovered only partially when the light was terminated ( $2.54 \pm 0.40$  Hz 5–20 min after termination of the stimulation; Wilcoxon signed rank test,  $Z = 2.92$ ,  $p = 0.004$ ). There was no significant reduction of firing rate in GFP control mice (before laser,  $2.83 \pm 0.90$  Hz; with laser,  $2.68 \pm 0.82$  Hz; Wilcoxon signed rank test,  $Z = 0.672$ ,  $p = 0.50$ ), suggesting that the rate reduction was not due to stimulation-induced tissue dysfunction. Laser stimulation caused a significant decrease in spatial information of the CA3 place cells (before laser,  $1.02 \pm 0.06$  bits/spike; with laser,  $0.74 \pm 0.06$  bits/spike, Wilcoxon signed rank test,  $Z = 4.32$ ,  $p = 1.5 \times 10^{-5}$ ; Figure 7C). There was no significant change in the size of the place fields as determined by population vector cross-correlation analysis (mean distance from diagonal to  $r = 0.2$  threshold before laser,  $3.41 \pm 0.49$  bins; with laser,  $4.00 \pm 0.35$  bins,  $p = 0.50$ ;  $p$  value was estimated from bootstrap distributions). There was also no change in the number of place fields ( $1.18 \pm 0.05$  versus  $1.22 \pm 0.07$ ; Wilcoxon signed rank test,  $Z = 0.435$ ,  $p = 0.664$ ).

Laser illumination led to a significant drop in spatial correlation between baseline and test trial (Figures 7D and 7E), comparable to the drop observed in animals with AAV-hM4D injections in the MEC (Figure 4; Tables S2 and S3). For cells that expressed place fields in both running directions, the amount of remapping, during laser application, was positively correlated between inbound and outbound place fields ( $R = 0.544$ ,  $p = 0.0023$ ), mirroring the results from the hM4D experiment. During the baseline trial, the rate maps were stable. In 75 out of 83 place fields (90%), the spatial correlation between the first half and the second half of the baseline session exceeded the 95<sup>th</sup> percentile of a shuffled distribution (Figure 7E). With laser application, only 30 of the 83 place fields (35%) passed the threshold

( $Z = 7.25$ ,  $p = 4.34 \times 10^{-13}$ , binomial test). 44 out of 83 place fields passed the threshold after termination of the laser stimulation. The decrease in the spatial correlation during laser illumination was significant (with laser versus baseline:  $r = 0.31 \pm 0.051$ ; first versus second half of the baseline:  $r = 0.81 \pm 0.014$ , paired sample t test for correlation values after Fisher z-transformation,  $t(82) = 9.37$ ,  $p = 1.06 \times 10^{-14}$ ). The spatial correlation with baseline showed some recovery after termination of the laser illumination ( $0.52 \pm 0.05$ , paired sample t test for correlation values after Fisher z-transformation compared with laser session  $t(82) = 4.73$ ,  $p = 9.00 \times 10^{-6}$ ). The drop in spatial correlations in the ArchT group was accompanied by a significant shift of the center of mass of place fields compared to the first versus second half of the baseline session ( $13.4 \pm 1.4$  cm versus  $7.3 \pm 1.6$  cm; Wilcoxon signed rank test,  $Z = 4.03$ ,  $p = 5.6 \times 10^{-5}$ ), as well as a drop in the population vector correlations. Whereas 20 out of 20 bins (100%) of the population vector correlations were outside of the 95<sup>th</sup> percentile of the shuffled distribution for the first versus the second half of the baseline trial, the number dropped to 15 (75%) for the comparison of light application and baseline ( $Z = 2.39$ ,  $p = 0.017$ , binomial test) (Figure 7E). The drop in the population vector correlations in the ArchT group was not significantly different from the drop with hM4D-mediated MEC inactivation (30 min post-CNO;  $0.18 \pm 0.02$  versus  $0.21 \pm 0.034$ , respectively;  $t(38) = 0.85$ ,  $p = 0.398$ ), but the decrease was significantly larger than when the light stimulation was applied in GFP control mice ( $0.87 \pm 0.10$ ;  $t(38) = 6.19$ ,  $p = 3.11 \times 10^{-7}$ ). Taken together, these results show that inactivation of dorsal MEC axons induces strong remapping in CA3 place cells.

As in the hM4D group, the change in spatial firing during laser stimulation was instantaneous. Population vectors were defined for each bin of each lap and correlated with the average vectors of the baseline session (Figure 6). We selected the last 10 laps

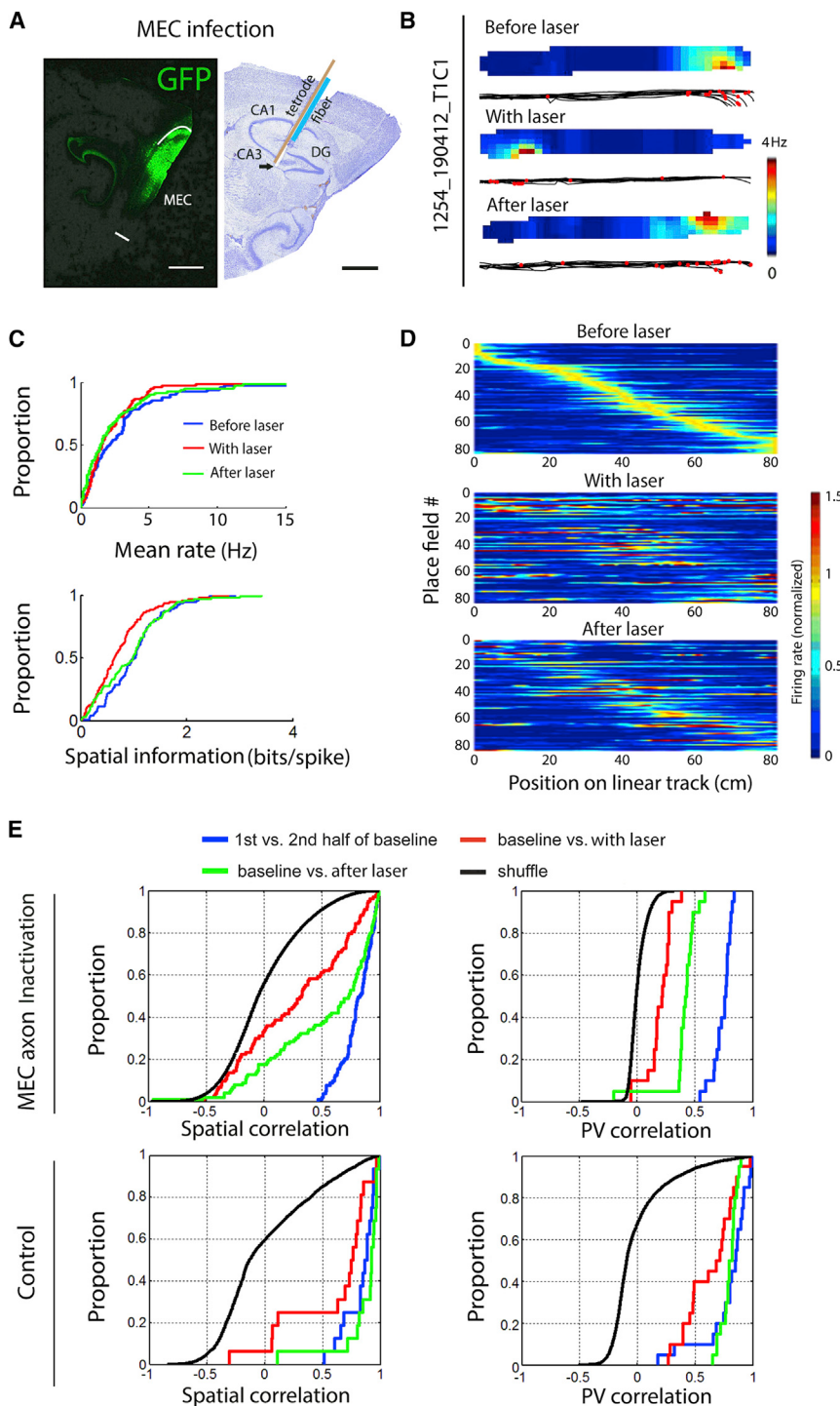


**Figure 7. Inactivation of Axons from MEC Induced Remapping in CA3 Place Cells**

(A) Left: sagittal brain section showing expression of ArchT-GFP(Green) protein in MEC. Dorsal and ventral borders of MEC are indicated by white lines. Scale bar, 800  $\mu$ m. Right: Nissl-stained sagittal brain section showing position of tetrode (arrow) and optical fiber in the hippocampus; symbols are as in Figure 2A.

(B) Example of CA3 place cells before, with, and after laser illumination.

(C) Cumulative frequency diagrams showing decreased mean firing rate and spatial information in place cells of ArchT-expressing animals during and after laser stimulation.

(D) Color-coded population map showing firing locations of CA3 place cells before, with, and after laser illumination ( $n = 83$ ). Symbols as in Figure 4A.

(E) Distribution of spatial correlations and population vector correlations for pairs of sessions in the laser experiment, as in Figure 4B.

first 10 laps with the laser was significantly higher than the correlation between the first lap with laser and the average of the 10 baseline laps ( $0.53 \pm 0.020$  versus  $0.25 \pm 0.024$ ,  $t$  test for correlation values after Fisher  $z$ -transformation,  $t(38) = 8.85$ ,  $p = 9.10 \times 10^{-11}$ ) (Figure 6C). Abrupt changes in firing patterns were not observed in GFP control animals with laser illumination (Figure 6D). The sudden transition of the population vector correlation on the first lap after laser onset is consistent with instantaneous remapping in the place-cell population.

Finally, remapping was not caused by retrograde transport of AAV to hippocampal neurons, since in 6 out of 8 mice there was no retrograde expression of ArchT in the hippocampus (Figures S3D–S3F). Although GFP-ArchT was seen in CA2 in 2 animals (Figures S4E–S4H), exclusion of these animals did not abolish the drop in spatial correlations after light application [first versus second half of baseline:  $0.81 \pm 0.02$ ; laser versus baseline:  $0.25 \pm 0.05$ ,  $t$  test for correlation values after Fisher  $z$ -transformation,  $t(70) = 10.2$ ,  $p = 1.96 \times 10^{-15}$ ; PV correlation of first versus second half of baseline:  $0.72 \pm 0.03$ ; PV correlation with laser

versus baseline:  $0.18 \pm 0.04$ ,  $t$  test for correlation values after Fisher  $z$ -transformation,  $t(38) = 11.0$ ,  $p = 2.39 \times 10^{-13}$ ] (Figure S7).

## DISCUSSION

This study reports two sets of observations. First, hippocampal place cells maintain their localized firing pattern after partial

from the baseline session and the first 10 laps from the laser session. The population vector correlation with the baseline average was significantly lower on the first lap after laser onset than on the last lap before the laser was turned on (before:  $0.55 \pm 0.031$ ; after:  $0.12 \pm 0.053$ ,  $t$  test for correlation values after Fisher  $z$ -transformation,  $t(38) = 6.94$ ,  $p = 2.94 \times 10^{-8}$ ). The correlation between the first lap with laser and the average of the

inactivation of the MEC. hM4D and ArchT were expressed across widespread regions of MEC, covering most of its dorso-lateral and mediolateral extent, but the intervention caused only minor changes in the size and shape of firing fields of place cells in the CA3 of the hippocampus. Second, while spatial firing was maintained, the distribution of firing locations was altered even after quite restricted silencing in the dorsal parts of MEC. Partial MEC inactivation caused substantial changes in hippocampal spatial representation at the neural ensemble level, reminiscent of the global remapping that occurs in place cells when animals move from one environment to another.

These findings have implications for the mechanisms of place-cell formation. The persistence of spatial firing despite widespread reduction in the firing rates of MEC neurons is consistent with results showing that a certain degree of localized firing is maintained in CA1 of animals with extensive bilateral lesions of the MEC, although the remaining firing fields are unstable (Miller and Best, 1980; Hales et al., 2014; Schlesiger et al., 2015). In the present study, MEC activity was decreased both instantaneously and reversibly, suggesting that the residual spatial firing was not caused by sprouting or other types of long-term compensatory reorganization known to take place in the hippocampus following entorhinal damage (Deller and Frotscher, 1997). The observations imply that localized firing can be generated in place cells by inputs from a wide range of afferent neurons, such that when a fraction, or even the majority, of these inputs is silenced, other spatial inputs may take over as determinants of firing locations in place cells. Following partial MEC inactivation, place fields may be generated by inputs from MEC cells whose firing rates were only partly reduced, or from spatially modulated cells in other parahippocampal regions including the parasubiculum and the lateral entorhinal cortex (Hargreaves et al., 2005; Boccaro et al., 2010). Finally, to some extent, localized firing likely mirrors the intrinsic ensemble structure of the hippocampus (Pastalkova et al., 2008; Villette et al., 2015).

Place fields may receive spatial information from a variety of cell types but the most prominent candidates in MEC are grid cells, border cells, and head direction cells (Hafting et al., 2005; Sargolini et al., 2006; Solstad et al., 2006), which each project to the hippocampus (Zhang et al., 2013). Two classes of models have been proposed for the transformation of information from these spatial cell types to place cells in the hippocampus. In the first class, place cells are formed by summation of inputs from either grid cells across a range of spatial frequencies (Fuhs and Touretzky, 2006; McNaughton et al., 2006; Solstad et al., 2006) or from border cells with variable distances from local borders in the environment (O'Keefe and Burgess, 1996; Hartley et al., 2000). This class of models requires a quite specific connection regime. In the second class of models, connections are largely random and different place cells receive, on average, more or less the same mix of inputs, with spatial selectivity arising in the hippocampus itself, either by local circuit computation (Monaco and Abbott, 2011; de Almeida et al., 2012) or via Hebbian plasticity (Rolls et al., 2006; Si and Treves, 2009; Savelli and Knierim, 2010). The present results show that place cells continue to fire at specific locations even after considerable changes in the balance of entorhinal inputs. There was no systematic change in the size of hippocampal place fields, contrary to predictions of simple versions of the linear

summation model for place field formation from grid cells. A similar lack of change in size of firing fields was apparent in another study that inactivated MEC cells with optogenetic methods (Rueckemann et al., 2015). Other studies using less confined inactivation methods have found a contraction of fields following large dorsal entorhinal lesions that extend into ventral entorhinal cortex (Van Cauter et al., 2008), or an expansion of fields following either dorsal or ventral entorhinal inactivation (Ormond and McNaughton, 2015) or selective lesions of layer III of MEC (Brun et al., 2008). The lesion or inactivation was more extensive and less specific in these latter studies than in the present one. With the lack of substantial and consistent changes in field size after regionally specific MEC inactivation, the present data, together with earlier and less specific work, speak in favor of an important intrahippocampal contribution to the refinement of spatial receptive fields. However, the detailed circuits and mechanisms, and the contribution of the various parahippocampal inputs, remain to be determined.

The most important finding of the present study is perhaps the observation that place cells remapped almost instantaneously after a change in the composition of MEC inputs to the hippocampus, caused by partial silencing in the MEC population. A similar shift in the distribution of place fields was observed when MEC was inactivated by local infusion of muscimol (Ormond and McNaughton, 2015, their Figure S8), although it was not clear from this study that the shift was instantaneous. In another study (Rueckemann et al., 2015), MEC cells were silenced optogenetically, but here the change in firing pattern was slow and gradual, not as expected if the mechanism was the same as when place cells remap under natural conditions (Muller and Kubie, 1987; Leutgeb et al., 2005b, 2006). In the present work, the transition to a new map was fully expressed already on the first lap of running. Moreover, the new firing pattern was maintained during the inactivation session, in the same way that firing remains stable following remapping after exposure to a new environment. While the cells maintained their ability to fire at specific locations, the distribution of firing rates and firing locations was altered to the extent that correlations with the original activity pattern overlapped considerably with that of a shuffled distribution, although the orthogonalization was not complete. A possible explanation of the different remapping patterns of the two studies is the recording location. Rueckemann et al. (2015) recorded in CA1, where cells are known to exhibit considerable hysteresis across successive experimental trials (Leutgeb et al., 2005a). The fast remapping observed in CA3 in the present work suggests that MEC inactivation can reproduce firing patterns of place cells that occur naturally in response to changes in MEC input when the environment is altered.

How the distribution of place fields is affected by signals from the MEC remains to be determined but the strong component of grid-cell input in the perforant-path projection to the hippocampus (Zhang et al., 2013) points to changes in firing patterns among grid cells as a major source of hippocampal remapping. Remapping may take place in the hippocampus in response to differential translations and rotations of firing maps across modules of grid cells (Fyhn et al., 2007; Stensola et al., 2012). When changes in the environment cause unequal changes in phase and orientation over grid modules, place cells will receive input

from new combinations of co-active grid cells. This in turn will change both the subset of place cells that pass the activation threshold and the location at which they are maximally activated (Stensola et al., 2012; Rowland and Moser, 2014). Determining the entorhinal firing patterns that cause remapping will eventually require interventions that target functional cell types specifically.

## EXPERIMENTAL PROCEDURES

### Subjects

The data were obtained from 26 male mice. The mice were 22–35 g at implantation. They were housed separately in transparent Plexiglass cages (35 cm × 30 cm × 30 cm) in a humidity- and temperature-controlled environment. All mice had tetrodes implanted in the right hippocampus or MEC. In two of the animals, tetrodes were implanted simultaneously in the hippocampus and the ipsilateral MEC. All animals were kept at 90% of free-feeding body weight and maintained on a 12-hr light/12-hr dark schedule. Testing occurred in the dark phase.

Virus with AAV5-CAG-ArchT-GFP, AAV2-hSyn-hM4D-mcitrine, AAV5-CAG-GFP, and AAV5-CAG-Tdtomato were from the University of North Carolina at Chapel Hill (UNC)'s gene therapy center. The titer of the virus was  $10^{12}$  viral genomic particles/ml. AAV5-CAG-ArchT-GFP and AAV5-CAG-GFP were from Edward Boyden's lab, Massachusetts Institute of Technology (MIT); AAV2-hSyn-hM4D-mcitrine was from Bryan Roth's lab, University of North Carolina at Chapel Hill (UNC). AAV2-CamKII-eArch3.0-EYFP was from Karl Deisseroth's lab, Stanford University. The titer of this virus was  $10^{13}$  viral genomic particles/ml.

Eight mice received injections of AAV5-CAG-ArchT-GFP, 15 mice received injections of AAV2-hSyn-hM4D-mcitrine, and two mice received injection of AAV2-CamKII-eArch3.0-EYFP. Testing of control animals (2 mice for the hM4D group and 1 for the ArchT group) was interleaved with testing of experimental groups. The experimenter was not blind to the identity of the animals.

### Surgery, Virus Injection, and Electrode Preparation

All animals were anesthetized with isoflurane (air flow: 0.8–1.0 l/min, 0.5%–3% isoflurane, adjusted according to physiological condition). The mice received subcutaneous injections of Bupivacaine (Marcaine) and buprenorphine (Temgesic) at the start of the surgery. Isoflurane was gradually reduced from 3% to 1%. Depth of anesthesia was examined by testing tail and pinch reflexes as well as breathing.

Upon induction of anesthesia, the animal was fixed in a Kopf stereotaxic frame for implantation. Holes for tetrode implantation were drilled in the skull above the right hippocampus and tetrodes were then implanted. The tetrodes were made of 17  $\mu\text{m}$  polyimide-coated platinum-iridium (90%–10%) wire. The electrode tips were plated with platinum to reduce electrode impedances to around 100–250 k $\Omega$  at 1 kHz. 22 mice received a microdrive (Axona) with two tetrodes. The tetrodes were inserted in the cortical surface 1.5–2.3 mm behind the bregma and 1.4–2.5 mm lateral to the midline. Four mice were implanted with a VersaDrive-4 (Neuralynx) with four tetrodes. The base of the VersaDrive-4 was modified to separate the tetrodes into two groups targeting MEC and hippocampus simultaneously. In the first group, two tetrodes were aimed at the right hippocampus (AP 1.5–2.3, ML 1.4–2.5) and in the second group two tetrodes were implanted above the ipsilateral MEC (0.35–0.40 mm anterior of the transverse sinus, 3.2–3.5 mm from midline, 1.5 mm below dura, 5 degree angle in the sagittal plane, with electrode tips pointing in the posterior direction). In ArchT-expressing animals, an optic fiber (lot number: MFC\_240/250-0.63\_16mm\_ZF1.25\_FLT, Doric) was implanted in the perforant-path termination zone in the hippocampus (AP 1.5–2.3, ML 1.4–2.5). Microdrives and optic fiber were secured to the skull with jewellers' screws and dental cement. Two front screws in the skull behind the eyes were connected to ground.

During the surgery, before the tetrodes were inserted, a 10- $\mu\text{l}$  NanoFil syringe (World Precision Instruments) and a 33G beveled metal needle was used for virus injection in MEC (0.4–0.35 mm anterior of the transverse sinus, 3.2–3.5 mm from midline, 1.2 mm below dura for dorsal injections, 2.5 mm below dura for ventral injections). Injection volume (0.5 to 1  $\mu\text{l}$  at each location)

and flow rate (0.1  $\mu\text{l}/\text{min}$ ) were controlled with a Micro4 Microsyringe Pump Controller (World Precision Instruments). After injection, the needle was left in place for 10 min before it was withdrawn slowly.

### Electrode Turning and Recording Procedures

Turning of tetrodes started 2 to 3 days after the surgery. Data collection began within 2 weeks. Before each recording session, the mice rested on a towel in a large flower pot on a pedestal. The mouse was connected to the recording equipment via AC-coupled unity-gain operational amplifiers close to the head and a counterbalanced cable that allowed the animal to move freely. Over the course of 20 to 30 days, the tetrodes were lowered in steps of 50  $\mu\text{m}$  or less, until well-separated single neurons could be recorded. When the signal amplitudes exceeded four times the noise level (20 to 30  $\mu\text{V}$ ), and single units were stable for more than 1 hr, data were collected.

Recorded signals were amplified 8,000 to 25,000 times and band-pass filtered between 0.8 and 6.7 kHz. Triggered spikes were stored to disk at 48 kHz (50 samples per waveform, 8 bits/sample) with a 32-bit time stamp (clock rate at 96 kHz). Electroencephalograms (EEG) were recorded single-ended from one of the electrodes. The local field potential was amplified 3,000 to 10,000 times, low-pass filtered at 500 Hz, sampled at 4,800 Hz, and stored with the unit data. Through a video camera, the recording system obtained the position of two light-emitting diodes (LEDs) on the headstage of the mouse. The LEDs were tracked individually at a rate of 50 Hz. The two LEDs were separated by 4 cm and aligned with the body axis of the mice.

Over the course of 3 to 6 weeks following surgery, the mice were first trained to run in a 1-m-square black aluminum enclosure polarized by a white cue card. In mice with putative border cells, the session in the square box was succeeded by a test in the same box with a 50-cm-long and 50-cm-high wall insert in the center of the box. These trials were 15 min. In parallel with training in the box, all mice were trained to run on a 1-m-long linear track. Running was motivated by randomly scattering crumbs of chocolate at 10 to 15 s intervals in the recording enclosure and by placing crumbs on alternating sides of the linear track before the conclusion of each lap. Each session lasted 10 to 15 min. On the linear track, the mice first ran 10 full laps (back and forth). In hM4d-expressing mice, this was followed by i.p. injection of 2 to 3 mg/kg of clozapine-N-oxide (CNO, Sigma). Thirty minutes later, the mice ran another 10 laps. A third session of 10 laps was conducted 12 hr after the injection. In ArchT-expressing mice, the baseline session was followed by 10 trials of continuous laser stimulation (532 nm) at a power density of 20 mW/mm<sup>2</sup> at the fiber tip. Five to 20 min after the laser was turned off, another 10 trials were conducted. There was no change in the running speed of the animals after laser stimulation (before:  $21.2 \pm 0.81$  cm/s; with laser:  $21.6 \pm 0.79$  cm/s, Wilcoxon signed rank test,  $Z = 0.013$ ,  $p = 0.99$ ). No signs of cell damage were seen in hippocampus after laser illumination (Figures S3G–S3I).

### Histological Procedures and Electrode Positions

The mice received an overdose of Equithesin and were perfused intracardially with saline followed by either 4% formaldehyde or 4% freshly depolymerized paraformaldehyde in phosphate buffer (PFA). The brains were extracted and stored in the same fixative, and frozen sagittal sections (30  $\mu\text{m}$ ) were cut and stained with cresyl violet. Each section through the relevant part of the hippocampus or MEC was collected for analysis. For LEC, only parts adjacent to MEC, i.e., the parts of LEC present in sections containing MEC, were collected and analyzed. All tetrodes were identified and the tip of each electrode was found by comparison with adjacent sections. Recordings from hippocampal tetrodes were included in the data analysis if the deepest position was in the CA3 pyramidal cell layer. The electrodes were not moved after recording.

For immunostaining, sections were rinsed 3 times for 10 min in 1× PBS (pH 7.6) at room temperature, preincubated for 2 hr in 10% normal goat serum in PBST (1× PBS with 0.5% Triton X-100). Between incubation steps, sections were rinsed in PBST. Sections were incubated either with antibodies against NeuN, raised in donkey (Millipore, 1:500), or GFP, raised in goat (Clontech, 1:2,000), or c-Fos, raised in goat (Calbiochem, 1:2,000), for 72 hr in anti-body-blocking buffer at 4°C. After three times of 15 min washing in PBST at room temperature, sections were incubated either in a mouse-anti donkey antibody or a rabbit-anti goat antibody conjugated with either fluorescein isothiocyanate or Cy3 (Jackson ImmunoResearch, 1:2,000) for 2 hr at room

temperature. After rinsing in PBS, sections were mounted onto glass slides with 4',6'-diamidino-2-phenylindole (DAPI)-containing Vectashield mounting medium (Vector Laboratories), and a coverslip was applied. Expression of hM4D or ArchT was estimated with anti-GFP, since a mCitrine or GFP tag was fused with hM4D or ArchT in the viral construct (GFP antibody also specifically binds with mCitrine). NeuN was used for staining neurons.

To examine the inhibition in mice injected with AAV-hM4D, we stained for the expression of the immediate-early gene *c-fos*. Animals were euthanized and perfused with cold PBS and 4% PFA, 30 min after injection of CNO. Sections for *c-fos* staining were acquired from 3 mice expressing AAV-hM4D and stained as described above. The number of *c-fos*-positive cells was determined with Image-Pro Plus software (Media Cybernetics). In each image, 5 of the 1 mm × 1 mm size windows were randomly selected to quantify the percentage of *c-fos*-positive cells that passed the threshold in MEC. The non-infected side was used as a control. Image-Pro Plus software was used for automatic counting of count *c-fos*-positive cells based on background optical density. Cells that surpassed 2× the background optic density were considered *c-fos* positive. The background optic density was established for each section in a nearby region lacking c-Fos.

To check for potential cell damage resulting from laser illumination, we used the TdT-mediated dUTP nick-end labeling (TUNEL) assay. Two mice were anesthetized and perfused and brains were dissected out and post-fixed for 24 hr in 4% PFA. The brains were cut and 20-μm-wide sections which were stored in PBS. The sections were mounted on poly-L-lysine (Sigma) coated slides, rehydrated by sequential incubations in 100%, 100%, 90%, 80%, 70% ethanol lasting 2 min each. The sections were then washed in 0.85% NaCl and PBS for 5 min each. Sections were fixed with 4% fresh PFA for 15 min and washed 3 times with PBS for 5 min each. The tissue was digested with 20 μg/ml Proteinase K (Amresco) solution for 10 min, washed with PBS, and then fixed with 4% PFA for 5 min, after which it was washed in PBS. For positive and negative control slides (from Abcam), cells were centrifuged and pipetted onto coated slides. The cells were fixed in 4% PFA when the slides were dry and washed three times in PBS, followed by 0.2% Triton X-100 (Sigma) solution for 5 min, after which they were washed in PBS. Apoptotic cells were detected using an *in situ* BrdU-Red DNA fragmentation (TUNEL) assay kit (Abcam) following the recommended standard protocol. The nuclei were labeled with Hoechst (Sigma) before mounting the sections with ProLong Gold Antifade solution (Invitrogen). The sections were imaged with a confocal microscope (Zeiss LSM 510).

#### Area of Virus Infection and Unfolded Maps

Unfoldings of MEC were prepared by mapping, for each sagittal brain section, the dorsal border of MEC onto a straight line. For each section, the surface length of MEC was measured with Image-Pro Plus software and subsequently mapped onto a straight line perpendicular to the line that represents the dorsal border. In order to assess the spread of the virus infection into areas adjacent to MEC, we also prepared unfolded maps of the postrhinal cortex, parasubiculum, presubiculum, lateral entorhinal cortex, and subiculum. In the case of postrhinal cortex, we used as a reference the ventral border, either with MEC or parasubiculum. For para- and presubiculum, the respective borders with MEC and subiculum were used. The lateral entorhinal cortex was aligned using its border with MEC, while for the subiculum, we used the border with CA1 as the alignment point in the map. Dorsal and ventral parts of the subiculum and of the pre- and parasubiculum were merged in these unfoldings. All borders were established using cytoarchitectonic criteria that can reliably be established irrespective of the plane of sectioning, as described in detail for the rat brain (Boccara et al., 2015). These borders, as defined in the rat, can be readily applied to the mouse brain (Witter, 2011). It is important to point out that in particular the mediolateral extent of parasubiculum, as well as that of postrhinal cortex, is extremely variable between individual animals. Cytoarchitectonic criteria, correlated to established chemoarchitectonic criteria, are therefore the only reliable way to establish those borders (Boccara et al., 2010, 2015). The percentage of the infected area on the unfolded map was taken as an indicator of the spread of hM4D or ArchT expression. Images of entorhinal cortex were scanned with an automated scanner (MIRAX MIDI, Carl Zeiss). Areas with GFP expression were considered as infected when the signal of GFP was

significantly higher than 2 SD of the mean value of the background signal with Image-Pro Plus software. The infected area surface was calculated with the same threshold for detection of the GFP signal.

#### Statistical Procedures

Pearson's correlation coefficients were calculated to estimate linear correlations between pairs of variables. We carried out Fisher z-transformations to decrease deviations from normality for parametric t tests. Non-parametric Wilcoxon or Mann-Whitney tests were used to assess differences of variables other than correlations. Significance levels were set as  $p < 0.05$  and are given for two-tailed tests. To estimate confidence intervals of population vector cross-correlations, we randomly sampled cell ensembles with replacement 500 times to obtain statistical distributions of correlations (bootstrap resampling method).

#### Approvals

Experiments were performed according to the Norwegian Animal Welfare Act and the European Convention for the Protection of Vertebrate Animals used for Experimental and Other Scientific Purposes. The experiments were approved by the National Animal Research Authorities of Norway.

#### SUPPLEMENTAL INFORMATION

Supplemental Information includes Supplemental Experimental Procedures, seven figures, and five tables and can be found with this article online at <http://dx.doi.org/10.1016/j.neuron.2015.09.051>.

#### AUTHOR CONTRIBUTIONS

C.M., E.I.M., and M.-B.M. designed research, C.M. and Q.C. collected data, C.M., Q.C., and H.T.I. analyzed data, M.W. helped with anatomy and histology, M.-B.M. and E.I.M. supervised the project, and C.M., H.T.I., Y.H., and E.I.M. wrote the paper with the input from all authors.

#### ACKNOWLEDGMENTS

We thank A.M. Amundsgård, K. Haugen, A. Burøy, E. Kråkvik, H. Waade, and V. Frolov for technical assistance. We thank Karl Deisseroth, Stanford University, for providing AAV2-CamKII-eArch3.0-EYFP virus. We thank Edward Boyden, MIT, for allowing us to use the vector AAV5-CAG-ArchT-GFP and Bryan Roth, UNC, for allowing us to use AAV2-Syna-hM4D-mCitrine. The work was supported by two Advanced Investigator Grants from the European Research Council ("ENSEMBLE"-grant agreement no. 268598; GRIDCODE-grant no. 338865), a grant from the European Commission's FP7 FET Proactive programme on Neuro-Bio-Inspired Systems (grant agreement 600725), a FRIPRO grant from the Research Council of Norway (grant no. 214164), the Centre of Excellence scheme of the Research Council of Norway (Centre for the Biology of Memory, grant number 145993; Centre for Neural Computation, grant number 223262), the Louis Jeantet Prize, the Körber Prize, and the Kavli Foundation.

Received: March 24, 2015

Revised: July 15, 2015

Accepted: September 23, 2015

Published: November 4, 2015

#### REFERENCES

- Alme, C.B., Miao, C., Jezek, K., Treves, A., Moser, E.I., and Moser, M.-B. (2014). Place cells in the hippocampus: eleven maps for eleven rooms. *Proc. Natl. Acad. Sci. USA* **111**, 18428–18435.
- Armbruster, B.N., Li, X., Pausch, M.H., Herlitze, S., and Roth, B.L. (2007). Evolving the lock to fit the key to create a family of G protein-coupled receptors potently activated by an inert ligand. *Proc. Natl. Acad. Sci. USA* **104**, 5163–5168.

- Battaglia, F.P., and Treves, A. (1998). Attractor neural networks storing multiple space representations: A model for hippocampal place fields. *Phys. Rev. E Stat. Phys. Plasmas Fluids Relat. Interdiscip. Topics* 58, 7738–7753.
- Boccaro, C.N., Sargolini, F., Thoresen, V.H., Solstad, T., Witter, M.P., Moser, E.I., and Moser, M.-B. (2010). Grid cells in pre- and parasubiculum. *Nat. Neurosci.* 13, 987–994.
- Boccaro, C.N., Kjønigsen, L.J., Hammer, I.M., Bjaalie, J.G., Leergaard, T.B., and Witter, M.P. (2015). A three-plane architectonic atlas of the rat hippocampal region. *Hippocampus* 25, 838–857.
- Brun, V.H., Leutgeb, S., Wu, H.-Q., Schwarcz, R., Witter, M.P., Moser, E.I., and Moser, M.-B. (2008). Impaired spatial representation in CA1 after lesion of direct input from entorhinal cortex. *Neuron* 57, 290–302.
- Chow, B.Y., Han, X., Dobry, A.S., Qian, X., Chuong, A.S., Li, M., Henninger, M.A., Belfort, G.M., Lin, Y., Monahan, P.E., and Boyden, E.S. (2010). High-performance genetically targetable optical neural silencing by light-driven proton pumps. *Nature* 463, 98–102.
- Colgin, L.L., Moser, E.I., and Moser, M.-B. (2008). Understanding memory through hippocampal remapping. *Trends Neurosci.* 31, 469–477.
- de Almeida, L., Idiart, M., and Lisman, J.E. (2012). The single place fields of CA3 cells: a two-stage transformation from grid cells. *Hippocampus* 22, 200–208.
- Deller, T., and Frotscher, M. (1997). Lesion-induced plasticity of central neurons: sprouting of single fibres in the rat hippocampus after unilateral entorhinal cortex lesion. *Prog. Neurobiol.* 53, 687–727.
- Eichenbaum, H. (2000). A cortical-hippocampal system for declarative memory. *Nat. Rev. Neurosci.* 1, 41–50.
- Ferbinteanu, J., and Shapiro, M.L. (2003). Prospective and retrospective memory coding in the hippocampus. *Neuron* 40, 1227–1239.
- Frank, L.M., Brown, E.N., and Wilson, M. (2000). Trajectory encoding in the hippocampus and entorhinal cortex. *Neuron* 27, 169–178.
- Fuhs, M.C., and Touretzky, D.S. (2006). A spin glass model of path integration in rat medial entorhinal cortex. *J. Neurosci.* 26, 4266–4276.
- Fyhn, M., Hafting, T., Treves, A., Moser, M.-B., and Moser, E.I. (2007). Hippocampal remapping and grid realignment in entorhinal cortex. *Nature* 446, 190–194.
- Hafting, T., Fyhn, M., Molden, S., Moser, M.-B., and Moser, E.I. (2005). Microstructure of a spatial map in the entorhinal cortex. *Nature* 436, 801–806.
- Hales, J.B., Schlesiger, M.I., Leutgeb, J.K., Squire, L.R., Leutgeb, S., and Clark, R.E. (2014). Medial entorhinal cortex lesions only partially disrupt hippocampal place cells and hippocampus-dependent place memory. *Cell Rep.* 9, 893–901.
- Han, X., Chow, B.Y., Zhou, H., Klapoetke, N.C., Chuong, A., Rajimehr, R., Yang, A., Baratta, M.V., Winkle, J., Desimone, R., and Boyden, E.S. (2011). A high-light sensitivity optical neural silencer: development and application to optogenetic control of non-human primate cortex. *Front. Syst. Neurosci.* 5, 18.
- Hargreaves, E.L., Rao, G., Lee, I., and Knierim, J.J. (2005). Major dissociation between medial and lateral entorhinal input to dorsal hippocampus. *Science* 308, 1792–1794.
- Hartley, T., Burgess, N., Lever, C., Cacucci, F., and O'Keefe, J. (2000). Modeling place fields in terms of the cortical inputs to the hippocampus. *Hippocampus* 10, 369–379.
- Igarashi, K.M., Lu, L., Colgin, L.L., Moser, M.-B., and Moser, E.I. (2014). Coordination of entorhinal-hippocampal ensemble activity during associative learning. *Nature* 510, 143–147.
- Ito, H.T., Zhang, S.J., Witter, M.P., Moser, E.I., and Moser, M.B. (2015). A pre-frontal-thalamo-hippocampal circuit for goal-directed spatial navigation. *Nature* 522, 50–55.
- Jarosiewicz, B., and Skaggs, W.E. (2004). Hippocampal place cells are not controlled by visual input during the small irregular activity state in the rat. *J. Neurosci.* 24, 5070–5077.
- Kentros, C.G., Agnihotri, N.T., Streater, S., Hawkins, R.D., and Kandel, E.R. (2004). Increased attention to spatial context increases both place field stability and spatial memory. *Neuron* 42, 283–295.
- Komorowski, R.W., Manns, J.R., and Eichenbaum, H. (2009). Robust conjunctive item-place coding by hippocampal neurons parallels learning what happens where. *J. Neurosci.* 29, 9918–9929.
- Leutgeb, S., Leutgeb, J.K., Treves, A., Moser, M.-B., and Moser, E.I. (2004). Distinct ensemble codes in hippocampal areas CA3 and CA1. *Science* 305, 1295–1298.
- Leutgeb, J.K., Leutgeb, S., Treves, A., Meyer, R., Barnes, C.A., McNaughton, B.L., Moser, M.-B., and Moser, E.I. (2005a). Progressive transformation of hippocampal neuronal representations in "morphed" environments. *Neuron* 48, 345–358.
- Leutgeb, S., Leutgeb, J.K., Barnes, C.A., Moser, E.I., McNaughton, B.L., and Moser, M.-B. (2005b). Independent codes for spatial and episodic memory in hippocampal neuronal ensembles. *Science* 309, 619–623.
- Leutgeb, S., Leutgeb, J.K., Moser, E.I., and Moser, M.-B. (2006). Fast rate coding in hippocampal CA3 cell ensembles. *Hippocampus* 16, 765–774.
- Markus, E.J., Qin, Y.L., Leonard, B., Skaggs, W.E., McNaughton, B.L., and Barnes, C.A. (1995). Interactions between location and task affect the spatial and directional firing of hippocampal neurons. *J. Neurosci.* 15, 7079–7094.
- McNaughton, B.L., Barnes, C.A., and O'Keefe, J. (1983). The contributions of position, direction, and velocity to single unit activity in the hippocampus of freely-moving rats. *Exp. Brain Res.* 52, 41–49.
- McNaughton, B.L., Battaglia, F.P., Jensen, O., Moser, E.I., and Moser, M.-B. (2006). Path integration and the neural basis of the 'cognitive map'. *Nat. Rev. Neurosci.* 7, 663–678.
- Miller, V.M., and Best, P.J. (1980). Spatial correlates of hippocampal unit activity are altered by lesions of the fornix and endorhinal cortex. *Brain Res.* 194, 311–323.
- Monaco, J.D., and Abbott, L.F. (2011). Modular realignment of entorhinal grid cell activity as a basis for hippocampal remapping. *J. Neurosci.* 31, 9414–9425.
- Muller, R.U., and Kubie, J.L. (1987). The effects of changes in the environment on the spatial firing of hippocampal complex-spike cells. *J. Neurosci.* 7, 1951–1968.
- Muller, R.U., Kubie, J.L., Bostock, E.M., Taube, J.S., and Quirk, G.J. (1991). Spatial firing correlates of neurons in the hippocampal formation of freely moving rats. In *Brain and Space*, J. Paillard, ed. (Oxford University Press), pp. 296–333.
- Nadel, L., Samsonovich, A., Ryan, L., and Moscovitch, M. (2000). Multiple trace theory of human memory: computational, neuroimaging, and neuropsychological results. *Hippocampus* 10, 352–368.
- O'Keefe, J. (1976). Place units in the hippocampus of the freely moving rat. *Exp. Neurol.* 51, 78–109.
- O'Keefe, J., and Burgess, N. (1996). Geometric determinants of the place fields of hippocampal neurons. *Nature* 381, 425–428.
- O'Keefe, J., and Dostrovsky, J. (1971). The hippocampus as a spatial map. Preliminary evidence from unit activity in the freely-moving rat. *Brain Res.* 34, 171–175.
- O'Keefe, J., and Nadel, L. (1978). *The Hippocampus as a Cognitive Map* (Oxford University Press).
- O'Keefe, J., and Speakman, A. (1987). Single unit activity in the rat hippocampus during a spatial memory task. *Exp. Brain Res.* 68, 1–27.
- Ormond, J., and McNaughton, B.L. (2015). Place field expansion after focal MEC inactivations is consistent with loss of Fourier components and path integrator gain reduction. *Proc. Natl. Acad. Sci. USA* 112, 4116–4121.
- Pastalkova, E., Itskov, V., Amarasingham, A., and Buzsáki, G. (2008). Internally generated cell assembly sequences in the rat hippocampus. *Science* 321, 1322–1327.

- Pavlides, C., and Winson, J. (1989). Influences of hippocampal place cell firing in the awake state on the activity of these cells during subsequent sleep episodes. *J. Neurosci.* 9, 2907–2918.
- Rolls, E.T., Stringer, S.M., and Elliot, T. (2006). Entorhinal cortex grid cells can map to hippocampal place cells by competitive learning. *Network* 17, 447–465.
- Rowland, D.C., and Moser, M.-B. (2014). From cortical modules to memories. *Curr. Opin. Neurobiol.* 24, 22–27.
- Rueckemann, J.W., DiMauro, A.J., Rangel, L.M., Han, X., Boyden, E.S., and Eichenbaum, H. (2015). Transient optogenetic inactivation of the medial entorhinal cortex biases the active population of hippocampal neurons. *Hippocampus*. Published online August 24, 2015. <http://dx.doi.org/10.1002/hipo.22519>.
- Sargolini, F., Fyhn, M., Hafting, T., McNaughton, B.L., Witter, M.P., Moser, M.-B., and Moser, E.I. (2006). Conjunctive representation of position, direction, and velocity in entorhinal cortex. *Science* 312, 758–762.
- Savelli, F., and Knierim, J.J. (2010). Hebbian analysis of the transformation of medial entorhinal grid-cell inputs to hippocampal place fields. *J. Neurophysiol.* 103, 3167–3183.
- Schlesiger, M.I., Cannova, C.C., Boubil, B.L., Hales, J.B., Mankin, E.A., Brandon, M.P., Leutgeb, J.K., Leibold, C., and Leutgeb, S. (2015). The medial entorhinal cortex is necessary for temporal organization of hippocampal neuronal activity. *Nat. Neurosci.* 18, 1123–1132.
- Scoville, W.B., and Milner, B. (1957). Loss of recent memory after bilateral hippocampal lesions. *J. Neurol. Neurosurg. Psychiatry* 20, 11–21.
- Si, B., and Treves, A. (2009). The role of competitive learning in the generation of DG fields from EC inputs. *Cogn. Neurodyn.* 3, 177–187.
- Solstad, T., Moser, E.I., and Einevoll, G.T. (2006). From grid cells to place cells: a mathematical model. *Hippocampus* 16, 1026–1031.
- Solstad, T., Boccara, C.N., Kropff, E., Moser, M.-B., and Moser, E.I. (2008). Representation of geometric borders in the entorhinal cortex. *Science* 322, 1865–1868.
- Squire, L.R. (1992). Memory and the hippocampus: a synthesis from findings with rats, monkeys, and humans. *Psychol. Rev.* 99, 195–231.
- Stensola, H., Stensola, T., Solstad, T., Frøland, K., Moser, M.-B., and Moser, E.I. (2012). The entorhinal grid map is discretized. *Nature* 492, 72–78.
- Van Cauter, T., Poucet, B., and Save, E. (2008). Unstable CA1 place cell representation in rats with entorhinal cortex lesions. *Eur. J. Neurosci.* 27, 1933–1946.
- Villette, V., Malvache, A., Tressard, T., Dupuy, N., and Cossart, R. (2015). Internally recurring hippocampal sequences as a population template of spatiotemporal information. *Neuron* 88, 357–366.
- Wilson, M.A., and McNaughton, B.L. (1994). Reactivation of hippocampal ensemble memories during sleep. *Science* 265, 676–679.
- Witter, M.P. (2011). The hippocampus. In *The Mouse Nervous System*, G. Paxinos, L. Puilles, and C. Watson, eds. (Academic Press), pp. 112–139.
- Wood, E.R., Dudchenko, P.A., Robitsek, R.J., and Eichenbaum, H. (2000). Hippocampal neurons encode information about different types of memory episodes occurring in the same location. *Neuron* 27, 623–633.
- Zhang, S.-J., Ye, J., Miao, C., Tsao, A., Cerniauskas, I., Ledergerber, D., Moser, M.-B., and Moser, E.I. (2013). Optogenetic dissection of entorhinal-hippocampal functional connectivity. *Science* 340, 1232627.